Composite Structures 94 (2012) 540–547

Contents lists available at SciVerse ScienceDirect

Composite Structures

journal homepage: www.elsevier.com/locate/compstruct

Damage and failure in low energy impact of fiber-reinforced polymeric composite laminates

R.C. Batra [a,*], G. Gopinath [a], J.Q. Zheng [b]

[a] Department of Engineering Science and Mechanics, M/C 0219, Virginia Polytechnic Institute and State University, Blacksburg, VA 24061, USA
[b] Program Executive Office, US Army, 15395 John Marshall Highway, Haymarket, VA 20169, USA

ARTICLE INFO

Article history:
Available online 22 August 2011

Keywords:
Damage
Failure
Elastoplastic deformations
Impact

ABSTRACT

We analyze the damage initiation, damage progression, and failure during 3-dimensional (3-D) elasto-plastic deformations of a fiber reinforced polymeric laminated composite impacted by a low speed rigid sphere, and compare computed results with experimental findings available in the literature. Damage is assumed to initiate when one of Hashin's failure criteria is satisfied, and its evolution is modeled by an empirical relation proposed by Matzenmiller, Lubliner and Taylor. The transient nonlinear problem is solved by the finite element method (FEM). Contributions of the work include considering damage in 3-D rather than plane stress deformations of a laminated structure and elasto-plastic deformations of the composite. This has been accomplished by developing a user defined subroutine and implementing it in the FE software ABAQUS. From strains supplied by ABAQUS the material subroutine uses a micro-mechanics approach based on the method of cells and values of material parameters of constituents to calculate average stresses in an FE, and checks for Hashin's failure criteria. If damage has initiated in the material, the subroutine evaluates the damage developed, computes resulting stresses, and provides them to ABAQUS. The damage evolved at a material point is not allowed to decrease during unloading. The delamination failure mode is simulated by using the cohesive zone model available in ABAQUS. The computed time histories of the axial load acting on the impactor are found to agree well with the experimental ones available in the literature, and various damage and failure modes agree qualitatively with those observed in tests.

1. Introduction

Composite laminates composed of fiber-reinforced plies are being increasingly used in automotive, aerospace, and defense industries because of their higher specific strength than those of metallic parts, and they can be engineered to obtain optimal material properties in desired directions. A challenging issue in designing composites is delineating various failure modes, such as fiber breakage, matrix cracking, fiber/matrix debonding, fiber kinking, and delamination between adjacent plies. The difficulty of the problem is evidenced by the fact that in the worldwide exercise summarized in [1] very few theories successfully predicted failure of composite coupons deformed quasistatically. In general, the load carrying capacity of a structure does not vanish as soon as either failure or damage ensues at a material point and the structure can support additional load before it eventually fails. Thus it is important to quantify damage caused by the initiation of a failure mode and study its development and progression and the eventual failure of a structure with an increase in the applied load. For designing impact resistant composite laminates it is important to understand energy dissipated in each failure mode.

Failure and damage in laminated structures can be studied by either using a micro-mechanics approach that considers failure and damage at the constituent level or a continuum damage mechanics (CDM) approach in which material properties of the composite have been homogenized and failure and damage is studied at the ply/lamina level; e.g., see [32–40]. Damage studied at the constituent level is not only computationally expensive for a real size problem but also requires extensive experimental characterization to determine values of material parameters in the damage model. For example, Togho and Weng [2] have used a statistical approach based on Weibull's distribution of inclusions and the assumption that the inclusion carries no load after it has debonded from the matrix; they thus included the effect of fiber/matrix debonding in Mori–Tanaka's micromechanics method of deriving effective properties. In Sun et al.'s [3] micromechanics-approach the effect of progressive debonding is considered by gradually reducing the elastic constants of the inclusions. Nguyen et al. [4] modeled the debonding process by reducing strengths of the interface between the inclusion and the matrix. Meraghni et al. [5] and

* Corresponding author.
E-mail address: rbatra@vt.edu (R.C. Batra).

0263-8223/$ - see front matter © 2011 Elsevier Ltd. All rights reserved.
doi:10.1016/j.compstruct.2011.08.015

Desrumaux et al. [6] have studied combined effects of micro-cracks and debonding on the effective properties of a composite.

One way to overcome the aforementioned limitation is to use a micromechanics approach to deduce effective properties of a ply and CDM to study failure and damage at the lamina level. We have adopted this hybrid technique to analyze the response of a laminated composite plate to low energy impacts. We note that Soden et al. [1] list numerous references describing failure theories and their predictive capability, and refer the reader to [1] for most of the literature on this subject. In the analysis of failure/damage of composites (e.g., see [1]) the inelastic behavior is often ignored. In low velocity impacts, damage and failure occur primarily due to bending stresses in the laminate [20] and the inelastic behavior of the matrix should not be neglected. The significance of considering inelastic deformations will become clear from results presented in the paper.

CDM theories capture effects of microscopic damage by using the theory of internal variables [7]. Ladeveze and Dantec [8] have used this approach to degrade elastic properties of the composite due to fiber breakage and matrix cracking, and a plasticity theory to account for permanent deformations induced under shear loading. Hassan and Batra [9] have used three internal variables to characterize damage due to fiber breakage, matrix cracking and fiber/matrix debonding. The delamination between adjacent plies was analyzed by using a failure surface quadratic in the transverse normal and the transverse shear stresses. Puck and Schurmann [10] have generalized Hashin's [11] stress-based failure criteria, and have proposed techniques to degrade elastic parameters of the lamina subsequent to the initiation of a failure mode. Donadon et al. [12] have used a smeared crack approach to develop a failure model for predicting damage in three-dimensional (3-D) deformations of a composite structure. Clegg et al. [13] have considered plastic deformations of a composite by assuming a yield surface quadratic in stresses, and have defined a damage surface in terms of stresses to consider damage induced softening. The evolution of damage variables is expressed in terms of a critical strain, fracture energy, fracture stress and a local characteristic dimension which should help minimize the dependency of computed results upon the finite element (FE) mesh used to numerically solve a problem. Ma and Cheng [14] have employed the Ramberg–Osgood plasticity relation to account for nonlinear response of a composite under in-plane shear loads, and considered fiber breakage, matrix cracking and interface debonding while studying the initiation and propagation of damage in a composite plate with a circular hole.

Matzenmiller et al. [15] have proposed that when one of Hashin's failure criteria is satisfied at a point in a composite structure, damage ensues at that point and it can be characterized by introducing internal variables for fiber breakage in tension and compression, matrix cracking in tension and compression, and crushing. The evolution of these internal variables depends upon values of stresses in Hashin's failure criteria which are expressed in terms of stress invariants for a transversely isotropic body and the strength parameters for the composite. Values of damage variables depend upon values of the five internal variables, and determine values of material elastic constants. Alternatively, the damage variables can be used to modify the six stress components used to characterize subsequent deformations of the material point. Xiao et al. [16] used this approach to study damage during quasistatic punching of woven fabric composites, and Williams and Vaziri [17] for studying damage in carbon fiber reinforced plastics under impact loads.

Here we use Matzenmiller et al.'s [15] damage evolution criteria for studying 3-D deformations of a 16-ply laminate impacted at normal incidence by a slow moving rigid sphere, and derive effective elasto-plastic properties of the composite by using Aboudi's [19] method of cells but with the continuity of shear tractions across cell boundaries relaxed (e.g., see [18]). The matrix is assumed to deform elasto-plastically and fibers elastically. A user defined subroutine has been developed and implemented in the commercial FE software ABAQUS that takes as input from ABAQUS values of the six strain components at an integration point of a FE, computes strains and stresses in each constituent by using the constituent level properties, computes effective stresses, checks for Hashin's failure criteria, computes damage if necessary, modifies stresses due to the induced damage, and supplies them to ABAQUS. In ABAQUS values of stresses suffice to find forces due to internal deformations. Accelerations of material particles are computed from the difference between the applied forces and forces due to internal stresses. The delamination between adjacent plies is characterized by using the cohesive zone model (CZM) available in ABAQUS. The computed time histories of the axial force experienced by the sphere, and the initiation and the propagation of failure modes agree qualitatively with experimental results of Curson et al. [20]. Thus contributions of the work include analyzing 3-D deformations of composite laminates under low energy impacts considering various damage and failure modes, and plastic deformations of the matrix.

2. Problem formulation

We refer the reader to Hughes's book [31] and ABAQUS manuals [23] for the derivation of a weak formulation of a transient problem, and to [24] for details of the numerical solution of the nonlinear problem studied herein. We briefly describe below the damage and the failure criteria.

2.1. Damage and failure criteria

Hashin [11] assumed that a fiber-reinforced ply can be modeled as a homogeneous linear elastic transversely isotropic body with the fiber axis as the axis of transverse isotropy, and proposed that the failure initiates when one of the five indices $f_\alpha(\alpha = 1,2,3,4,5)$ just exceeds 1.0.

Fiber tensile/compressive failure and lamina crush:

$$(f_1)^2 \equiv \left(\frac{\bar\sigma_{11}}{X_T}\right)^2 + \frac{\bar\sigma_{12}^2+\bar\sigma_{13}^2}{S^2}, \quad \bar\sigma_{11} > 0;$$

$$f_2 \equiv \frac{|\bar\sigma_{11}|}{X_C}, \quad \bar\sigma_{11} < 0; \qquad f_3 \equiv \frac{|\bar\sigma_{33}|}{Z_C}, \quad \bar\sigma_{33} < 0. \tag{1a-c}$$

Matrix tensile/compressive failure:

$$(f_4)^2 \equiv \left(\frac{\bar\sigma_{22}+\bar\sigma_{33}}{Y_T}\right)^2 + \frac{\bar\sigma_{23}^2-\bar\sigma_{22}\bar\sigma_{33}}{S_T^2} + \frac{\bar\sigma_{12}^2+\bar\sigma_{13}^2}{S^2}, \quad (\bar\sigma_{22}+\bar\sigma_{33}) > 0;$$

$$(f_5)^2 \equiv \left(\frac{Y_C}{2S_T}-1\right)^2\left(\frac{\bar\sigma_{22}+\bar\sigma_{33}}{Y_C}\right) + \left(\frac{\bar\sigma_{22}+\bar\sigma_{33}}{4S_T}\right)^2 + \frac{\bar\sigma_{23}^2-\bar\sigma_{22}\bar\sigma_{33}}{S_T^2} + \frac{\bar\sigma_{12}^2+\bar\sigma_{13}^2}{S^2}, \quad (\bar\sigma_{22}+\bar\sigma_{33}) < 0. \tag{1e}$$

Here $\bar\sigma_{ij}$ is the stress component with respect to the material principal axes of the ply, X_T (X_C) the axial tensile (compressive) strength along the $\bar x_1$-axis, Z_C the lamina crush strength, Y_T (Y_C) and S_T, respectively, the transverse tensile (compressive) strengths along the $\bar x_2$-axis and the shear strengths in the $\bar x_2\bar x_3$-plane with fibers aligned along the $\bar x_1$-axis. The shear strength in either the $\bar x_1\bar x_3$-plane or the $\bar x_1\bar x_2$-plane is denoted by S. We note that fiber failure due to kinking and buckling are not considered here.

Matzenmiller et al. [15] postulated that when an f_α in Eq. (1a–e) just exceeds 1 at a material point, the damage initiates there, and the material point loses its load carrying capacity when the

accumulated damage reaches a critical value. The damage evolution at a material point is defined in terms of an internal variable Q_α (α = 1, 2, 3, 4, 5) associated with the failure index f_α by the following empirical relation:

$$Q_\alpha = 1 - \exp\left[\frac{1}{m}(1-f_\alpha)\right], \quad (\alpha = 1,2,3,4,5); \qquad f_\alpha \geq 1. \tag{2}$$

A large (small) value of m implies that the damage evolves quickly (slowly), and the value of m is chosen by trial and error because of the unavailability of test data.

Instead of degrading values of elastic parameters at a point due to the damage evolved, one can enhance values of stresses there because the effective area supporting surface tractions is less than the geometric area. That is,

$$\hat{\boldsymbol{\sigma}} = \mathbf{D}\boldsymbol{\sigma}, \quad \hat{\bar{\boldsymbol{\sigma}}} = \mathbf{D}\bar{\boldsymbol{\sigma}} \tag{3a, b}$$

$$\langle D\rangle = \left\langle (1-\omega_1)^{-1}, (1-\omega_2)^{-1}, (1-\omega_3)^{-1}, (1-\omega_4)^{-1}, (1-\omega_5)^{-1}, (1-\omega_6)^{-1} \right\rangle \tag{4}$$

$$\omega_1 = \omega_5 = \mathrm{Max}(Q_1, Q_2, Q_3), \quad \omega_2 = \omega_4 = \mathrm{Max}(Q_3, Q_4, Q_5),$$
$$\omega_3 = Q_3, \quad \omega_6 = \mathrm{Max}(Q_1, Q_2, Q_3, Q_4, Q_5). \tag{5a-f}$$

Here **D** is a diagonal matrix, and the right-hand side of Eq. (4) gives diagonal elements of **D**. Furthermore, $\boldsymbol{\sigma}$ is written as a 6-D vector $\{\sigma_{11}, \sigma_{22}, \sigma_{33}, \sigma_{23}, \sigma_{13}, \sigma_{12}\}$. The motivation for definitions (5a–f) of the damage variables $\omega_1, \omega_2, \ldots, \omega_6$ is given in [22].

The irreversibility of the internal variable is accounted for by requiring that $dQ_\alpha = 0$ whenever $df_\alpha \leqslant 0$ where df_α represents an increment in f_α for an increment in the applied load. Eq. (5a–f) implies that more than one failure index influences the value of a damage parameter; for example, the value of Q_3 affects all six components of the damage vector ω. Thus even if an internal variable does not increase, the value of a damage parameter may increase. The effect of the damage evolved on subsequent deformations of a material point and on the value of the failure index f_α is considered by replacing $\bar{\boldsymbol{\sigma}}$ in Eqs. (1a–e) by $\hat{\bar{\boldsymbol{\sigma}}}$. The forces due to internal stresses are evaluated by using $\hat{\boldsymbol{\sigma}}$ rather than $\boldsymbol{\sigma}$.

An element is assumed to have failed when at least one of the five damage variables $Q_1, Q_2, \ldots, Q_5$ exceeds 0.95 *and* either the ratio of its final volume to the initial volume is less than 0.1 or more than 4.0 or the axial strain along the fiber direction equals at least 5%; e.g., see [16].

2.2. Elasto-plastic deformations of the matrix

We assume that fibers deform elastically and the matrix elasto-plastically, and plastic deformations of the polymer (PEEK) obey the von Mises yield criterion and the associated flow rule. The flow stress for the polymer depends upon the effective plastic strain to account for strain hardening.

3. Numerical results and discussion

The composite laminates studied are AS4/PEEK with 60% volume fraction of fibers, E_1 = 234 GPa, $E_2 = E_3$ = 14 GPa, $G_{12} = G_{13}$ = 27.6 GPa, G_{23} = 5.6 GPa, $\nu_{12} = \nu_{13}$ = 0.2, ν_{23} = 0.25 for the fiber and E = 4 GPa, ν = 0.35 for the matrix. Values of strength parameters in Hashin's failure initiation criteria obtained from the test data of [26] are: X_T = 1.4 GPa, X_C = 1.1 GPa, Y_T = 0.08 GPa, Y_C = 0.21 GPa, Z_C = 3.0 GPa, $S_T = S$ = 0.07 GPa, and m = 100 in Eq. (2). The value of the crush strength, Z_C, has not been widely reported in the literature, and values as high as 10 GPa have been used [27]. Here we have used Z_C = 3 GPa. A flat thin laminate impacted normal to the face sheet by a low speed sphere usually does not fail due to crushing; thus the precise value of Z_C is not critical for our work.

Goldberg and Stouffer [25] have reported experimental uniaxial stress–strain curve for the PEEK tested by Bordonaro [28] at 10^{-6}/s strain rate. For a given value of the axial stress, σ_{11}, the value of the axial plastic strain, ε_{11}^p, is computed from the relation, $\varepsilon_{11}^p = \varepsilon_{11} - \frac{\sigma_{11}}{E}$.

Points $(\varepsilon_{11}^p, \sigma_{11})$ are plotted and a least squares fit to these data points with a regression coefficient of 0.98 is

$$\bar{\varepsilon}^p = \exp\left(\frac{\bar{\sigma} - A}{N}\right) \qquad \text{for } 94 \text{ MPa} \geq \bar{\sigma} \geq 40 \text{ MPa}, \tag{6}$$

where A = 153 MPa and N = 13.86 MPa. Here $\bar{\sigma}$ and $\bar{\varepsilon}^p$ equal, respectively, the effective stress and the effective plastic strain.

4. Comparison of computed and experimental results

4.1. Simple quasi-static deformations

Since plastic deformations of the matrix play a dominant role when the laminate is deformed in simple shear in the x_1x_2-plane, computed results for this case with the specimen assumed to deform homogeneously are compared in Fig. 1 with the corresponding experimental results. The developed subroutine, VUMAT, implemented in the commercial FE software ABAQUS is used. It is clear that the computed results agree well with the experimental ones till a shear strain of 4% when the specimen failed in the tests. The computed shear strain, 5.2%, at failure exceeds the experimental value by 30%. The vertical drop in the stress shown for the experimental curve is our concoction and was not captured in experiments.

We now simulate Weeks and Sun's [21] experiments involving uniaxial loading of a lamina with unidirectional fibers inclined at an angle θ to the loading axis. Results presented in Fig. 2 for three values of θ clearly show that, prior to the onset of failure, the computed axial stress versus axial strain curves agree well with the corresponding experimental ones. The maximum difference between the computed and the experimental values of the axial strain at failure is less than 20%. One can again see that plastic deformations of the matrix significantly affect the stress–strain curves. We note that the stress to failure for both the elastic response and the elasto-plastic response is almost identical but there is considerable difference in the strain to failure, with the elasto-plastic response of the composite predicting results closer to the experimental values.

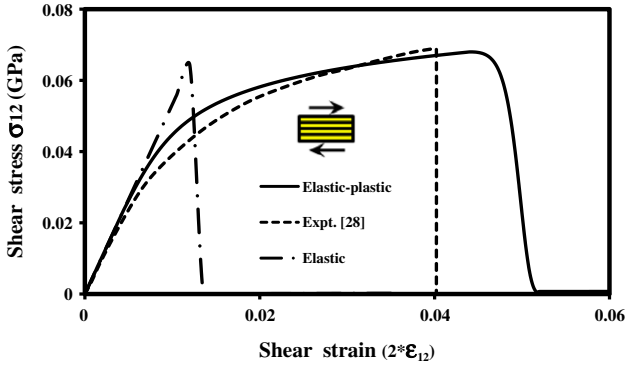

Fig. 1. Comparison of the experimental and the computed shear stress versus the shear strain curves for AS4/PEEK composite for shear deformations in the plane of the lamina.

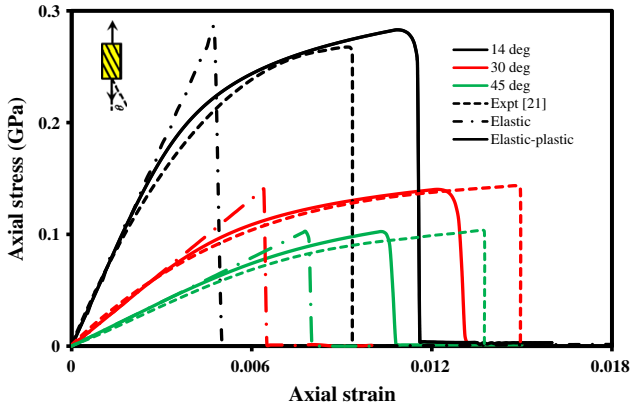

Fig. 2. Comparison of the experimental and the computed axial stress versus axial strain curves for AS4/PEEK composite for off-axis loading.

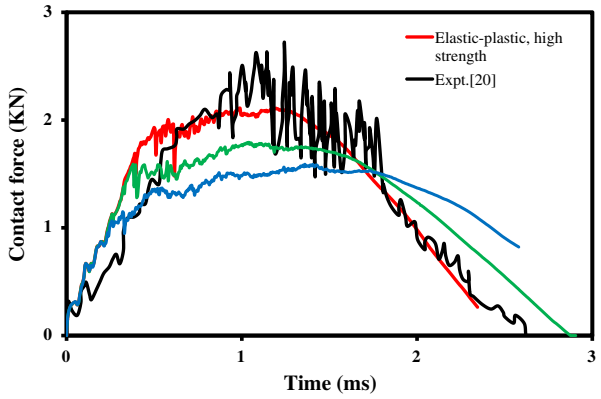

Fig. 4. Comparison of the computed and the experimental time histories of the contact force.

4.2. Impact loading of composite laminates

Fig. 3 shows a schematic sketch of the problem experimentally studied by Curson et al. [20] who delineated the response of 75 mm × 75 mm × 2 mm 16-layer $[-45/0/45/90]_{2S}$ AS4/PEEK composite laminates impacted at normal incidence by a 500 g 12.7 mm diameter steel sphere. Curson et al. [20] employed a hemi-spherical nosed cylindrical impactor and observed that it did not deform much; here we regard the impactor to be rigid. Since the contact area is anticipated to depend upon the radius of the hemi-spherical nose of the projectile, and the damage induced in the laminate upon the kinetic energy of the impactor, replacing the cylindrical projectile by a spherical one should not significantly affect the computed damage in the laminate.

As displayed in Fig. 3 the composite laminate is supported on a steel plate having a 50 mm diameter circular opening. Assumptions of modeling the sphere and the supporting plate as rigid are reasonable since the elastic modulus of steel is several orders of magnitude higher than that of the composite in the transverse direction. The coefficient of friction between the spherical impactor and the composite laminate is set equal to 0.25, and material parameters are assigned the following values: $X_N = 80$ MPa, $X_{S1} = X_{S2} = 150$ MPa. Values of the fracture energy $G_{IC} = 150$ J/m^2, $G_{IIC} = G_{IIIC} = 500$ J/m^2 and $\eta = 1.7$ used herein are typical for carbon fiber reinforced polymer composites [29]. There is, in general, considerable scatter in the literature values of strength parameters X_T and Y_T; for example, Curson et al. [20] reported $X_T = 2.1$ GPa and $Y_T = 0.135$ GPa which are higher than those used here.

We used the default values 0.06 and 1.2, respectively, for the linear and the quadratic artificial bulk viscosities, and of the penalty parameter in the "GENERAL CONTACT" algorithm included in ABAQUS EXPLICIT.

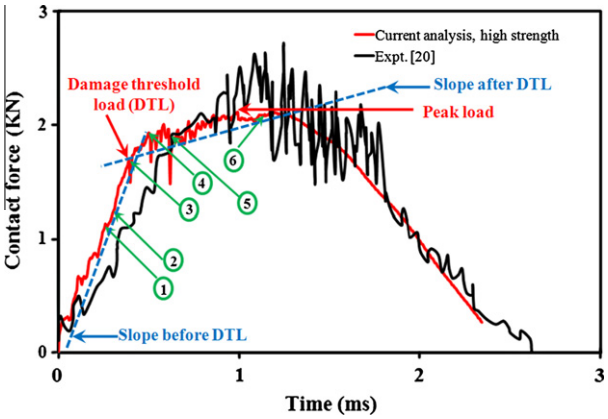

Fig. 5. Contact force time history plot with points of significance for the damage initiation and propagation.

For the initial velocity = 4 m/s of the sphere (initial kinetic energy = 4 J), we have compared in Fig. 4 the computed time history of the contact force, F_C (for both elastic and elasto-plastic response of the composite), with the experimental one. The time is reckoned from the instant of contact between the sphere and the laminate, and results have been computed for $(X_T, Y_T) = (1.04, 0.08)$ GPa and (2.1, 0.135) GPa for the elasto-plastic response and $(X_T, Y_T) = (1.04, 0.08)$ GPa for the elastic response. During the initial 0.25 ms of contact, the total computed force between the sphere and the laminate for each case is more than that measured experimentally. For the elasto-plastic response different values of (X_T, Y_T) have negligible effect on the magnitude of F_C and for $t > 0.25$ ms, the lower values of (X_T, Y_T) result in a smaller value of F_C. Also

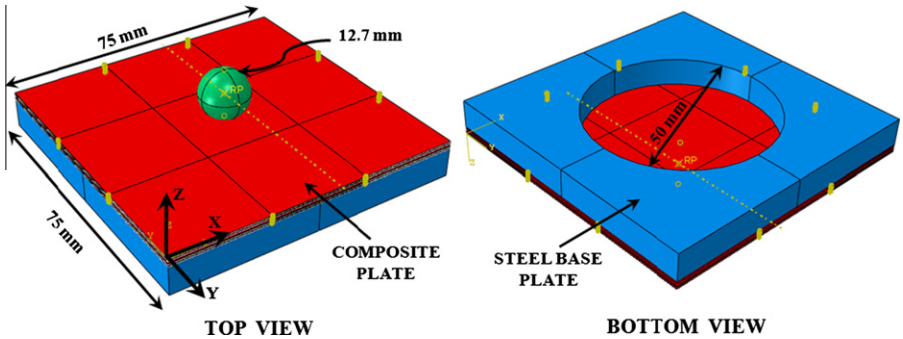

Fig. 3. Sketch of the impact problem studied with the impactor shown in green, the composite laminate in red, and the supporting steel plate in blue color. (For interpretation of the references to color in this figure legend, the reader is referred to the web version of this article.)

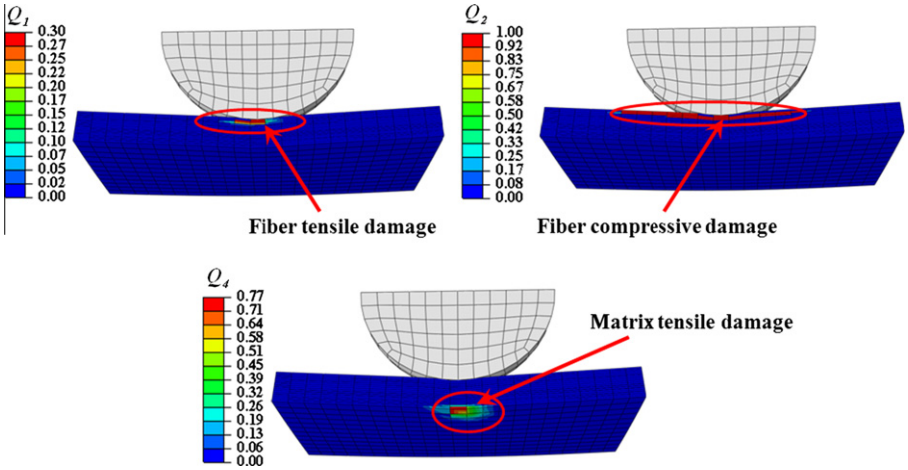

Fig. 6a. Fringe plots of internal variables Q_1 (fiber tensile damage), Q_2 (fiber compressive damage) and Q_4 (matrix tensile damage) at $t \approx 0.4$ ms.

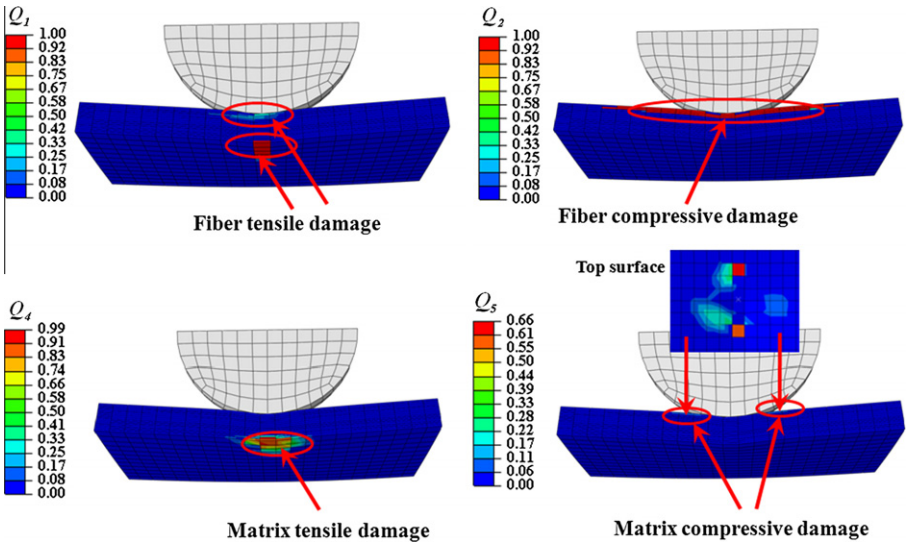

Fig. 6b. Fringe plots of internal variables Q_1 (fiber tensile damage), Q_2 (fiber compressive damage), Q_4 (matrix tensile damage) and Q_5 (matrix compressive damage) at $t \approx 0.52$ ms.

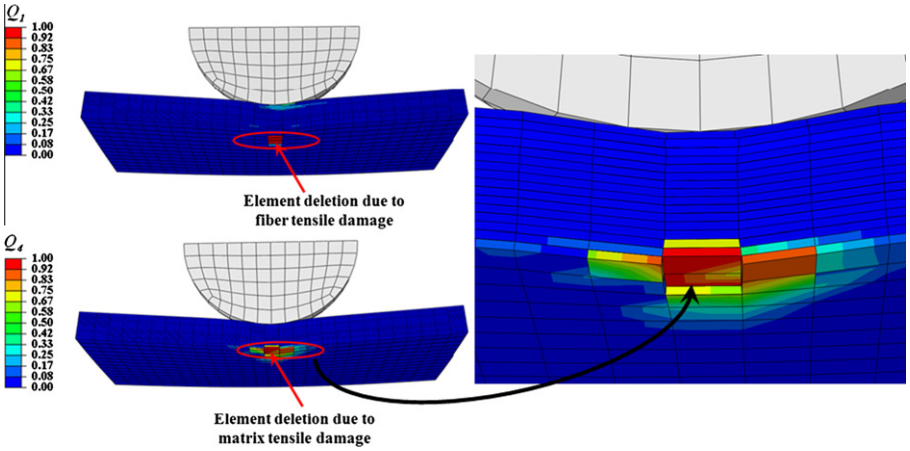

Fig. 6c. Fringe plots of internal variables Q_1 (fiber tensile damage) and Q_4 (matrix tensile damage) at $t \approx 0.55$ ms.

the time, t_p, when the two computed values of F_C peak agrees well with the corresponding experimental value. In the neighborhood of $t = t_p$ the amplitude of oscillations in the experimental values of F_C is considerably more than that in the computed values of F_C. The time, t_f, when the sphere looses contact with the laminate is the least for $(X_T,\ Y_T) = (2.1,\ 0.135)$ GPa and the most for $(X_T,\ Y_T) = (1.04,\ 0.08)$ GPa. The sphere remains in contact with the laminate for about 2.5 ms. The peak value of the contact force F_c for the elastic response of the composite has the lowest value. For the higher strength composite the slope of the unloading part of the curve is steeper than that for the lower strength composite.

4.3. Evolution of damage during impact loading

In Fig. 5 arrows pointing to different locations on the contact force time history plot refer to points of significance for the damage initiation and the damage evolution. The fiber compressive damage associated with the internal variable Q_2 initiates first at ~0.25 ms, and occurs at a point contacting the impactor; this is indicated as '1' in Fig. 5. The corresponding fringe plot of Q_2, shown in Fig. 3–13a of [24], suggests that the damage due to fiber compression is localized in a narrow region below the impactor and it does not affect the contact force. The matrix tensile damage, quantified by values of Q_4, initiates next at the bottom-most layer of the composite plate at ~0.3 ms after impact. It is indicated as point '2' in Fig. 5 and fringe plots of the fiber compressive and the matrix tensile damage are shown in Fig. 3–13b of [24]. The value of the fiber compressive damage variable has increased to nearly 1 but the damage remains localized at points below the impactor. The initiation of the two damage modes does not seem to influence the force between the impactor and the laminate. Even though the value of the internal variable has exceeded 0.95, the

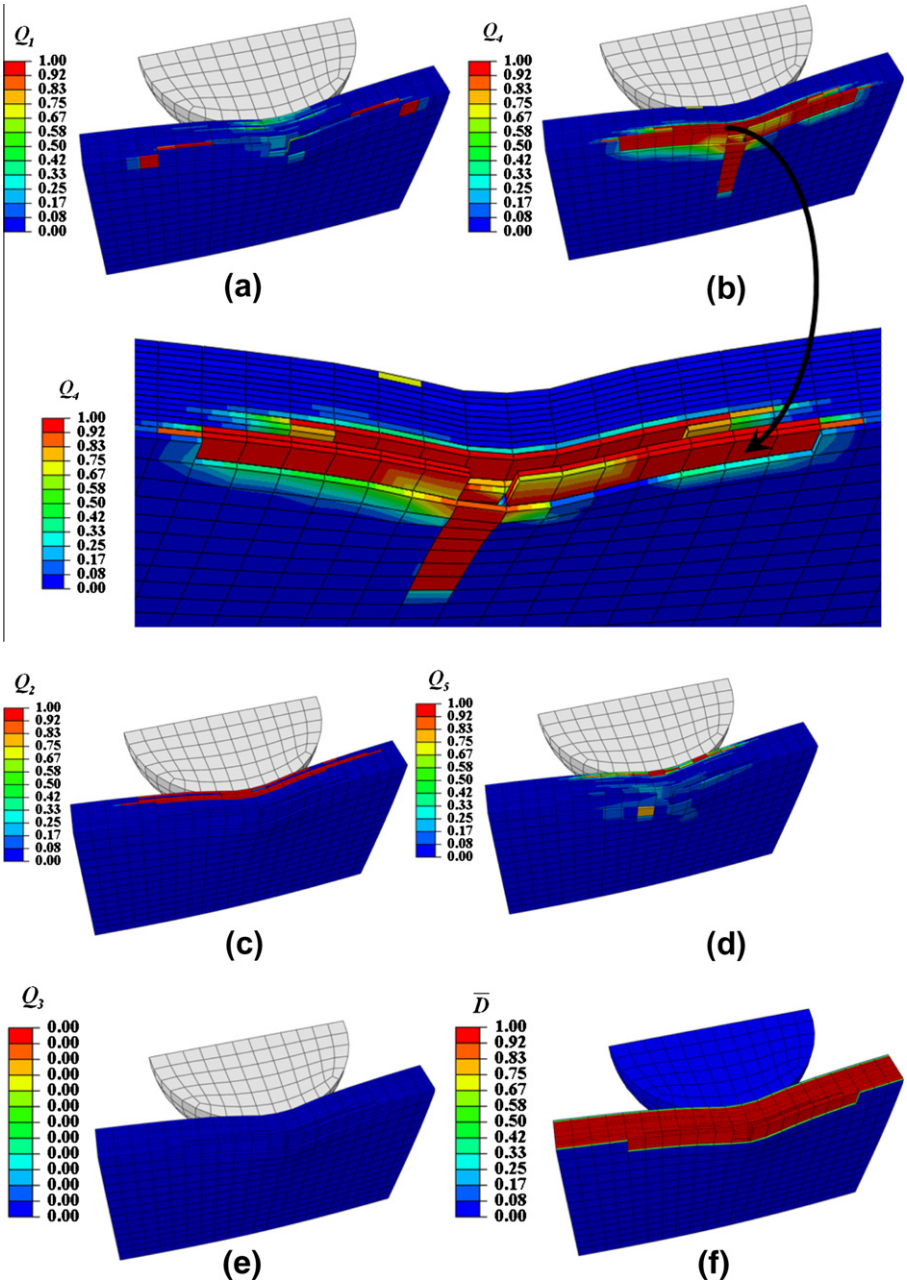

Fig. 7. (a–f): At $t = 1.1$ ms, fringe plots of internal variables (a, b) Q_1 and Q_4 associated with the fiber and the matrix tensile damage, (c, d) Q_2 and Q_5 associated with the fiber and the matrix compressive damage, and (e, f) Q_3 and $\bar{D}$ associated with crush damage and delamination.

other two auxiliary criteria for element deletion have not been satisfied.

The fiber tensile damage, signified by values of Q_1, initiates along the top-most layers of the composite plate at ~0.4 ms after impact and is indicated as point '3' in Fig. 5. The corresponding fringe plots for the three damage modes shown in Fig. 6a suggest that the matrix tensile damage has increased in the bottom layers of the laminate while the fiber compressive damage has spread out in the top layers of the laminate. Also noticeable in the contact force time history plot is a sharp drop in the contact force at this instant. This drop is attributed to both the fiber tensile damage and the growth of the fiber compressive and the matrix tensile damage modes. The drop in the contact force is followed by a further increase in the contact force but now at a rate less than that prior to the drop. Schoeppner and Abrate [30] called this point as the "damage threshold load" (DTL); it equals the impact load at which there is sufficient accumulation of damage in the composite plate causing a noticeable reduction in its stiffness and hence a change in the slope in the contact force time history plot.

The compressive matrix damage, decipherable from values of Q_5, initiates at $t \approx 0.45$ ms but is limited to points near the top surface of the composite plate. At $t \approx 0.52$ ms the second drop in the contact force is observed (indicated as '4' in Fig. 5). The fringe plot of the compressive damage mode shown in Fig. 6b indicates that the damage is insignificant to warrant a drop in the contact force. The fringe plot of the fiber tensile damage mode reveals that significant fiber tensile damage occurs in the bottom layers of the composite plate but the region of the fiber tensile damage has not grown in the top layers of the plate. The magnitudes of other damage modes have also not increased much. Hence it can be concluded that the second drop in the contact force at point '4' is due to the accumulation of the fiber tensile damage along the bottom layers of the composite laminate.

At $t \approx 0.55$ ms, indicated as point '5' in Fig. 5, we see another sharp drop in the contact force whose magnitude is much larger than that of the previous two drops in the contact force. Fringe plots of the internal variables Q_1 (fiber tensile damage mode) and Q_4 (matrix tensile damage mode) shown in Fig 6c indicate that elements have been deleted from the FE mesh which reduced the laminate stiffness and caused the contact force to drop. The other damage modes are primarily restricted to the top layers of the composite plate, and no element has been deleted in that region.

At $t = 1.1$ ms we have exhibited in Fig. 7 fringe plots of internal variables Q_1, Q_2, Q_3, Q_4, Q_5 and $\bar{D}$ that characterize damage due to fiber tensile failure, fiber compressive failure, laminate crushing, the matrix tensile failure, the matrix compressive failure, and the delamination between adjacent plies, respectively. In the magnified view of Fig. 7b one can see several elements that failed due to the matrix failing in tension and were deleted during the analysis. There are several elements directly underneath the spherical impactor in Fig. 7c in which the fibers failed due to the excessive axial compressive stress. Fringe plots of the internal variable, Q_3, associated with the crush damage shown in Fig. 7e reveal that there is no damage induced due to the laminate crushing. However, fringe plots of the damage variable, $\bar{D}$, displayed in Fig. 7f lead to the conclusion that the delamination between adjacent plies occurs over a very large region.

At $t \approx 1.25$ ms the impactor begins to rebound (indicated as point '6' in Fig. 5). A significant number of elements have failed by this time. The damage patterns and evolution of damage variables are similar to those described by Curson et al.

4.4. Effect of FE mesh size and rate of damage evolution

To see sensitivity of results to the FE mesh, we considered 3 element sizes, namely, 0.65 mm (mesh 1), 0.775 mm (mesh 2) and 0.96 mm (mesh 3); these dimensions are for elements that are in close vicinity of the impactor. The maximum size of an element along the outer edges of the lamina varies from 1 mm for mesh 1 to 1.25 mm for mesh 3. This gives approximately 120,000, 85,000 and 70,000 elements for meshes 1, 2 and 3, respectively. The contact force time history plots for the $[-45/0/45/90]_{2S}$ laminate for the three FE meshes, shown in Fig. 8 suggest that the mesh size has only a marginal effect on the contact force time history. Each of these FE meshes has only one element through a ply thickness.

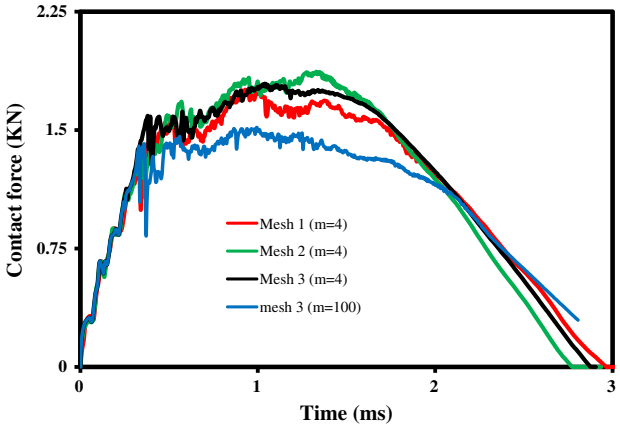

Fig. 8. Effect of mesh size and parameter m on the contact force time history plot.

The value of the parameter m in Eq. (2) determines how quickly the damage evolves. Whereas the shapes of the time history curves for $m = 4$ and $m = 100$ are very similar to each other, the peak contact force for $m = 100$ is considerably smaller than that for $m = 4$. Thus the choice of m determines the maximum computed contact force.

5. Discussion and conclusions

We have analyzed by the finite element method (FEM) transient elasto-plastic deformations of a fiber reinforced AS4/PEEK laminate impacted at normal incidence by a rigid sphere moving at a slow speed. The matrix is assumed to deform elasto-plastically and fibers elastically. The material properties of each FE in the composite are found by using a micromechanics approach, namely, the method of cells. Based on the stresses induced in the FE we find whether or not a failure mode has initiated by using Hashin's failure criteria. An internal variable is associated with each failure mode whose evolution is used to account for the irreversible damage induced in the FE. Thus values of material parameters of the constituents rather than those of the composite are needed. However, values of strength parameters for the composite are required. Hence we have coupled the continuum damage mechanics and micromechanics approaches to study failure and damage in fiber reinforced laminates. The usefulness and the validity of the approach have been demonstrated by solving a realistic impact problem.

The proposed hybrid approach predicts well different failure mechanisms in the laminated plate impacted by a slow moving rigid sphere. The computed time history of the total axial force acting on the impactor agrees well with the experimental one available in the literature. For the problem studied the delamination failure occurs over an extensive region beneath the spherical impactor. Fibers below the impactor fail in compression, and the matrix in the bottom-most plies fails in tension. A wide crack develops in the third ply from the bottom surface for the $[-45/0/45/90]_{2S}$ laminate. The predicted evolutions of the matrix and the fiber damage agree well with experimental observations of Curson et al. Furthermore, it is shown that the consideration of plastic deformations of the matrix significantly affects the contact force

experienced by the impactor. Also, the matrix may fail in tension before fibers fail pointing out the significance of the matrix strength.

Acknowledgments

This research was sponsored by the Army Research Laboratory (ARL) and was accomplished under Cooperative Agreement Number W911NF-06-2-0014. The views and conclusions contained in this document are those of the authors and should not be interpreted as representing official policies, either expressed or implied, of the ARL or the US Government. The US Government is authorized to reproduce and distribute reprints for Government purposes notwithstanding any copyright notation hereon. The work was also partially supported by the Office of Naval Research Grant N00014-1-06-0567 to Virginia Tech with Dr. Y.D.S. Rajapakse as the program manager. Views expressed herein are those of the authors and neither of the funding agencies nor of their institutions.

References

[1] Soden PD, Kaddour AS, Hinton MJ. Recommendations for designers and researchers resulting from the world-wide failure exercise. Compos Sci Technol 2004;64:589–601.
[2] Togho K, Weng GJ. A progressive damage mechanics in particle-reinforced metal-matrix composites under high tri-axial tension. J Eng Mater Technol 1994;116:414–20.
[3] Sun LZ, Ju JW, Liu HT. Elasto-plastic modeling of metal matrix composites with evolutionary particle de-bonding. Mech Mater 2003;35:559–69.
[4] Nguyen BN, Tucker BJ, Khaleel MA. A mechanistic approach to matrix cracking coupled with fiber–matrix de-bonding in short fiber reinforced composites. J Eng Mater Technol 2005;127:337–50.
[5] Meraghni F, Blakeman CJ, Benzeggah ML. Effect of interfacial decohesion on stiffness reduction in a random discontinuous-fiber composite containing matrix micro-cracks. Compos Sci Technol 1996;56:541–55.
[6] Desrumaux F, Meraghni F, Benzeggah ML. Micromechanical modeling coupled to a reliability approach for damage evolution prediction in composite materials. Appl Compos Mater 2000;7:231–50.
[7] Coleman BD, Gurtin M. Thermodynamics with internal variables. J Chem Phys 1967;47:597–613.
[8] Ladeveze P, Dantec ELe. Damage modeling of the elementary ply for laminated composites. Compos Sci Technol 1992;43:257–67.
[9] Hassan NM, Batra RC. Modeling damage in polymeric composites. Composites B 2008;39:66–82.
[10] Puck A, Schurmann H. Failure analysis of FRP laminates by means of physically based phenomenological models. Compos Sci Technol 2002;62:1633–62.
[11] Hashin Z. Failure criteria for unidirectional fiber composites. J Appl Mech 1980;47:329–34.
[12] Donadon MV, De. Almeida SFM, Arbelo MA, Faria AR. Three-dimensional ply failure model for composite Structures. Int J Aerospace Eng 2009;2009:1–22.
[13] Clegg RA, White DM, Riedelb W, Harwick W. Hypervelocity impact damage prediction in composites: Part I—material model and characterization. Int J Impact Eng 2006;33:190–200.
[14] Maa RH, Cheng JH. A CDM-based failure model for predicting strength of notched composite laminates. Composites B 2002;33:479–89.
[15] Matzenmiller A, Lubliner J, Taylor RL. A constitutive model for anisotropic damage in fiber composites. Mech Mater 1995;20:125–52.
[16] Xiao JR, Gama BA, Gillspie JW. Progressive damage and delamination in plain weave S-2 glass/SC-15 composites under quasi-static punch shear loading. Compos Struct 2007;78:182–96.
[17] Williams KV, Vaziri R. Application of a damage mechanics model for predicting the impact response of composite materials. Compos Struct 2001;79:997–1011.
[18] Robertson DD, Mall S. Micromechanical analysis for thermo-viscoplastic behavior of unidirectional fibrous composites. Compos Sci Technol 1994;50:483–96.
[19] Aboudi J. Mechanics of composite materials. Amsterdam: Elsevier Science Publication; 1991.
[20] Curson AD, Leach DC, Moore DR. Impact failure mechanisms in carbon Fiber/PEEK composites. J Thermoplast Compos Mater 1990;3:24–31.
[21] Weeks CA, Sun CT. Modeling non-linear rate-dependent behavior in fiber-reinforced composites. Compos Sci Technol 1998;58:603–11.
[22] MAT 162 user reference manual; 2005 <http://www.ccm.udel.edu/Tech/MAT162/MAT162Manual_v3.pdf>.
[23] ABAQUS 6.10 theory manual, <http://www.esm.vt.edu/v6.10/>.
[24] Gopinath G. Progressive damage and failure of unidirectional fiber reinforced laminates under impact loading with composite properties derived from a micro-mechanics approach, PhD, dissertation. Virginia Tech; 2011.
[25] Goldberg RK, Stouffer DC. Strain rate dependent analysis of a polymer matrix composite utilizing a micromechanics approach. J Compos Mater 2002;36:773–93.
[26] Kyriakides S, Arseculeratne R, Perry E, Liechti K. On the compressive failure of fiber reinforced composites. Int J Solids Struct 1995;32:689–738.
[27] Chan S, Fawaz Z, Behdinan K, Amid R. Ballistic limit prediction using a numerical model with progressive damage capability. Compos Struct 2007;77:466–74.
[28] Bordonaro CM. Rate dependent mechanical behavior of high strength plastics: experiment and modeling, PhD dissertation. Troy, New York: Rensselaer Polytechnic Institute; 1995.
[29] Turon A, Dávila CG, Camanho PP, Costa J. An engineering solution for mesh size effects in the simulation of delamination using cohesive zone models. Eng Fract Mech 2007;74:1665–82.
[30] Schoeppner GA, Abrate S. Delamination threshold loads for low velocity impact on composite laminates. Composites A 2000;31:903–15.
[31] Hughes TJR. The finite element method. Linear static and dynamic analysis. NJ: Prentice Hall; 1988.
[32] Batra RC, Hassan NM. Blast resistance of unidirectional fiber reinforced composites. Composites B 2008;39:513–36.
[33] Batra RC, Hassan NM. Response of fiber reinforced composites to underwater explosive loads. Composites B 2007;38:448–58.
[34] Kachanov L. On the creep rupture time. Izv Akad Nauk SSSR 1958;8:26–31.
[35] Rabotnov Y. On the equations of state for creep. Progress in applied mechanics. Prager Anniversary vol. New York: Macmillan; 1963.
[36] Talreja RA. Continuum mechanics characterization of damage in composite materials. Proc Royal Soc London 1985:399; 195–216.
[37] Ladeve'ze P. A damage computational method for composite structures. Comput Struct 1992;4:79–87.
[38] Barberis U, Hassim A, Ravera C, Vanderborck G. Impact-induced damage analysis tool for laminated composites. Advances in composite materials and structures VII. Boston: WIT Press; 2000.
[39] Krajcinovic D, Fonseka GU. The continuous damage theory of brittle materials. Part 1: General theory. J Appl Mech 1981;48:809–15.
[40] Carol I, Rizzi E, Willam K. On the formulation of anisotropic elastic degradation. Part I. Theory based on a pseudo-logarithmic damage tensor rate. Int J Solids Struct 1965;38:491–518.